Friction **11**(6): 894–910 (2023)
https://doi.org/10.1007/s40544-022-0627-4
ISSN 2223-7690
CN 10-1237/TH
RESEARCH ARTICLE

Investigations for vibration and friction torque behaviors of thrust ball bearing with self-driven textured guiding surface

Can WU[1], Kai YANG[1], Jing NI[1,*], Shuigen LU[2,3], Lidan YAO[4], Xinglin LI[2,3]

[1] *School of Mechanical Engineering, Hangzhou Dianzi University, Hangzhou 310018, China*

[2] *Hangzhou Bearing Test & Research Center with Assistance of UNDP/UNIDO, Hangzhou 310022, China*

[3] *Machinery Industry Bearing Quality Inspection Center (Hangzhou), Hangzhou 310022, China*

[4] *Sinopec Research Institute of Petroleum Processing, Beijing 100083, China*

Received: 04 July 2021 / Revised: 06 December 2021 / Accepted: 24 March 2022

Abstract: In order to improve the starved lubrication condition of rolling bearings, three kinds of textures, namely dimple, groove texture, and gradient groove texture, were developed on the guiding surface of thrust ball bearings in this study. The results show that gradient groove texture has the one-way self-driving function of liquid droplets. The root mean square (RMS) value of vibration acceleration of gradient groove textured bearing (GGB) decreased by 49.1% and the kurtosis decreased by 24.6% compared with non-textured bearing (NB) due to the directional spreading effect of gradient groove textures on oil. The frequency domain analysis showed that the textures mainly suppressed the medium and high-frequency energy of bearing vibration, and the GGB was reduced the most with 65.3% and 48%, respectively. In addition, whether the grease is sufficiently sheared has a large impact on the oil guiding effect, and the friction torque of GGB could decrease by 10.5% compared with NB in the sufficiently sheared condition. Therefore, the gradient groove texture with oil self-driven effect on the guiding surface of rolling bearing can effectively improve the lubrication condition of the bearing and thus reduce the bearing vibration and friction torque, which has a promising application prospect.

Keywords: self-driven textures; gradient grooved bearing (GGB); guiding surface; bearing vibration; friction torque

1 Introduction

Rolling bearings are the core components in the field of rotating machinery. According to statistics, about 90% of rolling bearings are lubricated by grease [1]. Therefore, how to improve the friction, wear, and lubrication state of rolling bearings has always been a hot topic for many scholars to explore. The existing research shows that most of the grease lubricated rolling bearings are under starved conditions in the normal operation process. This is due to the fact that the grease in the bearing raceway will be squeezed out of the raceway area and accumulate on the guiding surface when the rolling body runs, so that only a very small amount of grease is really involved in the bearing lubrication. This makes grease lubricated bearings under extreme conditions (high speed and high load), more likely to face the problems caused by starvation lubrication (lack of grease lubrication) [2], such as a significant reduction in the thickness of oil film in the contact area [3, 4]. It leads to higher friction and wear, which greatly reduces the service life of the bearing.

Since the 1960s, the effect of textures on contact surfaces has received increasing attention. In particular, the improvement of textures on friction, wear, and

* Corresponding author: Jing NI, E-mail: nijing2000@163.com

lubrication by surface micro-texture has been deeply studied in both academia and industry [5–7]. The current applications of textures on bearings are mainly focused on sliding bearings. Vlădescu et al. [8] and Fowell et al. [9] evaluated the effects of textures on journal bearings and found that friction reduction could be achieved even under extreme wear conditions. Tala-Ighil et al. [10] investigated the effect of texture location on the performance of plain bearings and concluded that the presence of surface texture enhances the oil film thickness at local contact locations to reduce friction. Ye et al. [11] and Marian et al. [12] proved that the textures can enhance the maximum load of the journal bearing.

However, the application of textures on rolling bearings is relatively rare. Bhardwaj et al. [13] tested the temperature rise, friction torque, and vibration performance of the thrust ball bearings having conventional and textured races. The results showed that the textures can reduce the friction torque of the bearings, and also the good grease retention effect in the textured area can improve the contact damping and reduce the bearing vibration. Vidyasagar et al. [14] used nanosecond pulsed laser to apply textures on the inner ring of deep groove ball bearings. The experiments showed that under light load, there was a significant reduction in friction torque and vibration, and the wear condition of the bearing raceway surface was improved. Hsu et al. [15] created a series of shallow (0.9/1.1 μm) periodic patterns on thrust rolling bearing raceways and proved that textured pockets could enhance the formation of anti-wear tribo-film. Their bearing fatigue lifetime evaluation results also shows that the texture has a positive effect on bearing life. The above research is to improve the rolling body/raceway rolling–sliding contact form by processing the microstructure in the bearing raceway, so as to improve the bearing performance. In the long-term operating of rolling bearings, the contact area is mostly under starved grease lubrication condition [2]. And a large amount of grease is squeezed and accumulated on the guiding surface by the rolling element, which do not participate in the lubrication of raceway contact area. If these grease or bleed oil can be guided into the raceway to participate in lubrication, the bearing performance will be greatly improved, which is also the starting point of this study.

In recent years, functional surface technologies have been developed in many fields, such as superhydrophobic surfaces [16], trapped light structured surfaces [17], antibacterial surfaces [18], and anti-corrosion surfaces [19], where the derived liquid self-driven technologies have gradually attracted great attention from related researchers. The wedge-patterned functional surface prepared by Deng et al. [20] enables the motion control of a single droplet. Li et al. [21] used a micro-sculpting method to prepare a topological liquid diode on a silicon wafer, which has a uniform arrangement of microstructures that allows the liquid to flow in one direction while the reverse of the motion is cut off. Liu et al. [22] designed silica surfaces with a wetting gradient to achieve the orientation and long-distance transport of water droplets. Chen et al. [23] achieved the high-speed unidirectional flow of water droplets by fabricating continuously adjustable gradient microstructures on Ti sample surface. Li et al. [24] prepared a functional surface composed of groove textures to achieve unidirectional spreading of oil and analyzed the self-transport mechanism of oil droplets. Liu et al. [25] prepared a periodic comb-tooth-shaped microstructures with unidirectional spreading guidance for oil droplets on steel and glass discs, respectively. The textured steel and glass discs were rotating in friction experiments and interferometry film thickness measurement tests (ball on disc model). The results show that the comb-tooth-shaped patterns can still maintain a good unidirectional replenishment of oil droplets to the contact area. The liquid self-driven technology is more widely applicable and less costly, and can be used to achieve unidirectional wetting of liquids on common metal surfaces.

Based on the above research, we designed and processed gradient groove micro-structure on thrust ball bearing guiding surface, which can realize the directional self-driven flow of lubricating fluid to the raceway. Meanwhile, dimples textures (isotropic) and uniform groove textures were set as the control group. And the research was carried out from three aspects: Wetting performance of textured surface, bearing vibration test, and friction torque test.

2 Experimental

2.1 Preparation of lithium complex grease

Lithium complex grease (LCG) was adopted in this experiment, and the preparation process is as follows: First, poly-alpha-olefin (PAO40) base oil (290 g), 12-hydroxystearic acid (45 g), and sebacic acid (15 g) were added into the reactor and heated to 90–100 °C for 30 min. Second, 100 g lithium hydroxide aqueous solution (12.5 g lithium hydroxide monohydrate and 87.5 g water) was added to make the material dehydrated and saponified. Then the reactor was gradually heated up to 200–210 °C. Third, PAO40 (150 g) was poured into the kettle and cool the mixture to 100 °C. Finally, the LCG sample was obtained by grinding initial grease twice through the three-roll mill. The percentage of lithium complex soap as thickener in the prepared LCG is 12 wt%. The basic physical properties of LCG and PAO40 are shown in Tables 1 and 2. Figure 1 shows the scanning electron microscopy (SEM) morphology of the LCG thickener. It can be seen that the LCG thickener is composed of slender nano-sized fibers, and the soap fibers are coiled and twisted to form a natural micro-gap [26].

2.2 Preparation of textured bearing

In order to ensure the consistency of the experiment, the same batch of NSK thrust ball bearings (NSK-51405) were purchased as the test bearings. According to ISO15242 (rolling bearings–measuring methods for vibration), four sets of NSK-51405 bearings were tested for bearing base vibration using PAO40 oil. The results show that the vibration of the four bearings remain consistent. As shown in Fig. 2, the test bearing consists of upper ring, lower ring, balls, and cage. The components of thrust ball bearings are easy to separate and assemble. In this way, repeated assembly in the process of texture machining and experiments will not cause damage to the bearing itself, thus avoiding the influence of bearing assembly/separation on the experimental results.

Table 1 Physical properties of LCG.

Grease	Thickener type	Oil	NLGI grade	Penetration (0.1 mm)
LCG	Complex lithium soap	PAO40	2	268

Table 2 Physical properties of PAO40.

		PAO40	Experimental method
Kinematic viscosity (mm^2/s)	40 °C	386	ASTM D445
	100 °C	40	
Viscosity index	—	147	ASTM D2207
Pour point (°C)	—	–40	ASTM D97
Flash point (°C)	—	295	ASTM D92

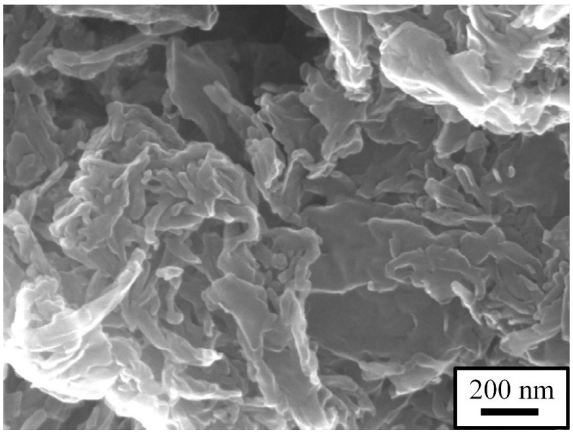

Fig. 1 SEM image of LCG thickener.

Laser etching technology was used to create textures on bearing guiding surface. The laser marking machine (Han's laser Technology Industry Group Co., Ltd.) was set up with an output power of 5 W, a repetition rate of 50 kHz, and an etching speed of 500 mm/s. The minimum line width of this equipment is 0.05 mm, and the repeatability is ±0.3 μm. Because the lower ring of thrust ball bearing rotates with the spindle, the centrifugal force will affect the flow of the bleed oil on the guiding surface toward the raceway, which will weaken the effect of the textured surface on the base oil [13]. In order to eliminate the influence of centrifugal force and facilitate the comparison of experimental results, three types of textures (dimple, groove, and gradient groove) were set on the guiding surface of upper ring that stayed unrotated. The diameter of the dimples is 150 μm, while the center distance is 550 μm. The dimples are arranged crosswise. The uniformly distributed grooves have a center distance of 180 μm and width of 50 μm. The gradient groove textured region is divided into seven regions in the gradient direction with increasing texture density. The minimum center distance of

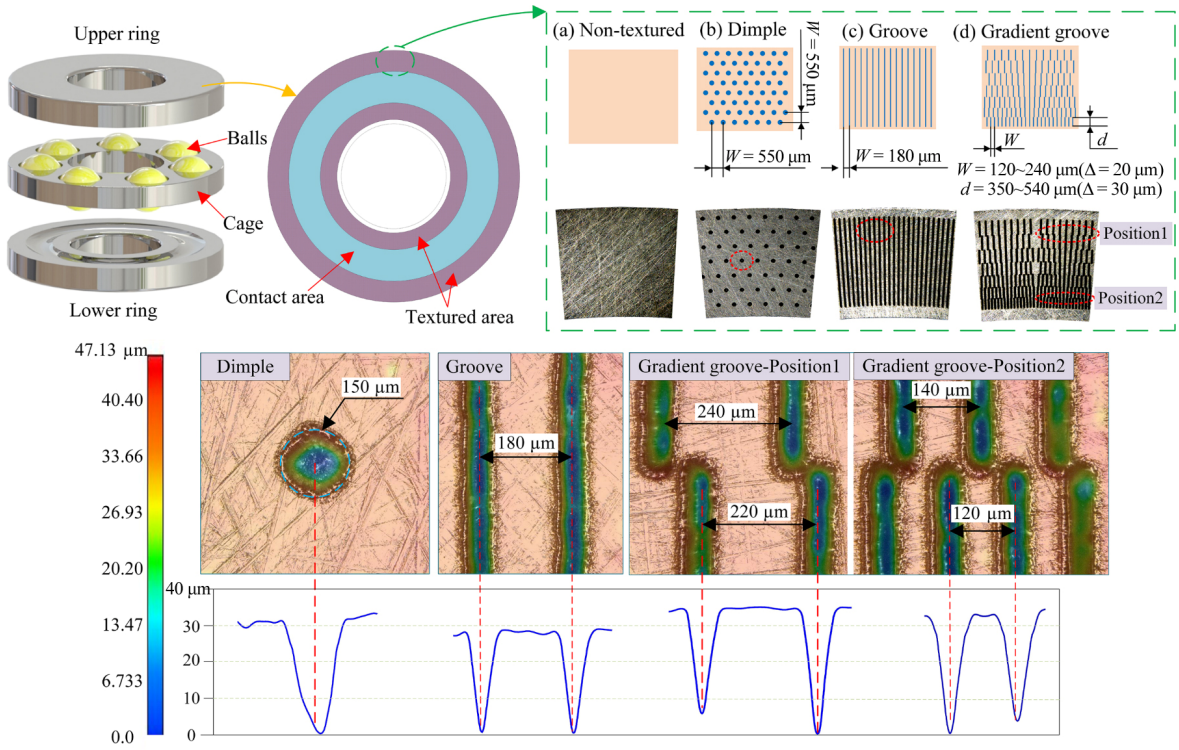

Fig. 2 Distribution and specific size of the texture on the guiding surface of the upper ring.

grooves is 120 μm, and the minimum length is 350 μm. In the two adjacent regions from high to low density, the groove center distance is increased by 20 μm and the length of grooves is increased by 30 μm. In addition, the depths of all textures are 30–40 μm. Overall, this paper would use non-textured bearing (NB), dimpled bearing (DB), grooved bearing (GB), and gradient grooved bearing (GGB) to conduct the experiments. The distribution and specific size of the texture on the guiding surface of the upper ring are shown in Fig. 2. Figure 3 shows SEM images of textured guiding surface.

2.3 Experimental process

2.3.1 *Bearing vibration test*

In this study, the vibration performances of test bearings were evaluated by BVT-7 bearing vibration tester as shown in Fig. 4. The upper ring is mounted in the clamp to keep it fixed, and the lower ring is installed on a hydrostatic spindle which is driven by the belt connected to the servo motor. Since the hydrostatic spindle is supported by liquid, the radial vibration of the hydrostatic spindle is less than 1/80 times that of the bearing vibration. Therefore, the

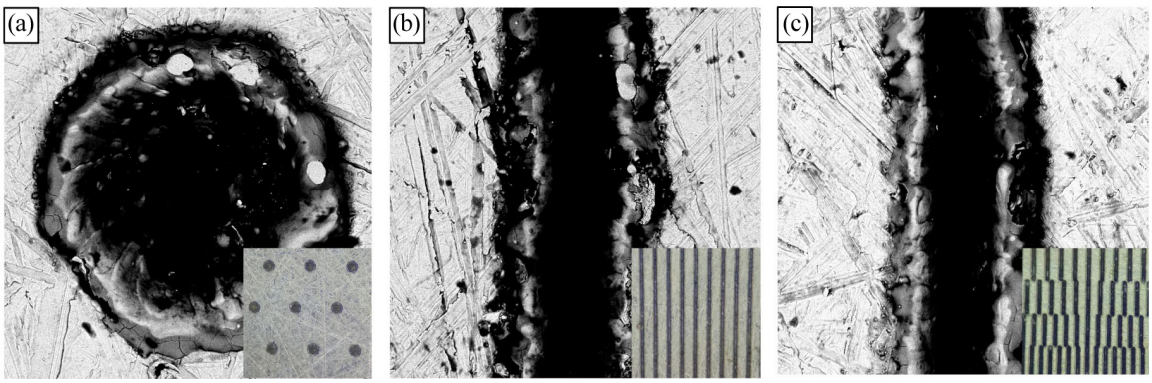

Fig. 3 SEM images of textured guiding surface: (a) DB, (b) GB, and (c) GGB

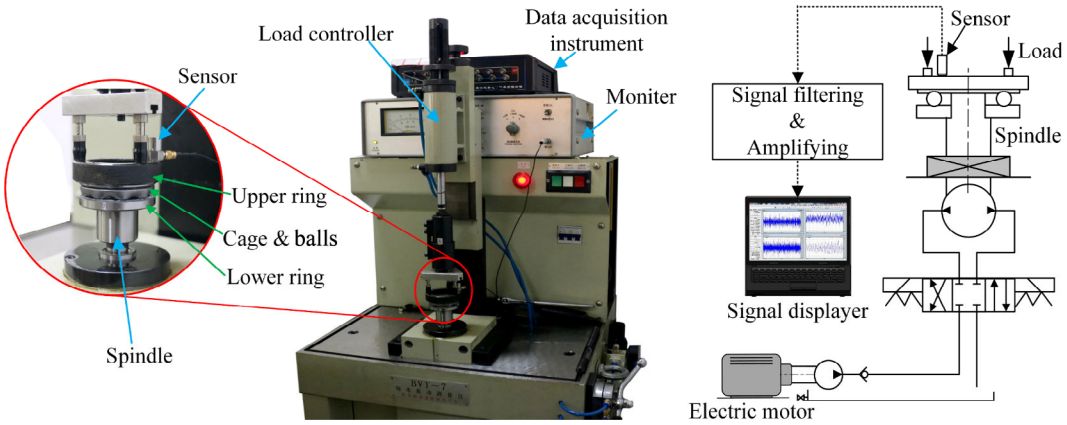

Fig. 4 Schematic diagram of BVT-7 bearing vibration tester.

misalignment of the two raceway axes caused by the spindle vibration is very small, which avoids the vibration caused by the radial sloshing of the thrust ball bearing. The axial loading part is driven by the air pump and loaded on the upper ring in the downward direction. The acceleration sensor is installed on the outer surface of the upper ring, and the axial vibration of the bearing could be collected by the sensor. In this experiment, the data acquisition instrument (uT3408FRS-ICP) was used to acquire the sensor signals and analysis software (uTekAcquV2.0 & uTekSsV2004) was applied to analyze the bearing acceleration signals. The sampling frequency was set to 10,240 Hz.

Bearing vibration tests were carried out under the driving spindle speed of 1,800 r/min and axial load of 220 N. The specific experimental procedures are as follows:

1) The upper and lower ring, cages, and steel balls of the test bearings were cleaned by petroleum ether solution in ultrasonic waves for 10 min and then naturally dried at room temperature.

2) To ensure the consistency of the experimental conditions, 2 mL grease (about 1/3 of inner free space of the bearing) was applied on the upper and lower rings uniformly by a syringe.

3) The upper and lower rings were installed on the fixture and hydraulic spindle respectively according to Fig. 4, and 220 N axial load was applied to the bearing.

4) Set the rotating speed to 1,800 r/min and start the test. In order to eliminate the influence of grease distribution in raceway on bearing vibration, the spindle runs for 5 min before data collection to make grease evenly distributed in the bearing. Until the vibration value of monitor tended to be stable, the bearing vibration acceleration data was collected every 1 min for 3 s, and a total of 8 sets of data were collected.

5) The upper and lower rings were carefully removed to avoid damaging the distribution of grease in the raceway. The grease fingers (finger-shaped grease) in the raceway were photographed by the Keyence VHC-1000C microscope.

2.3.2 *Friction torque test*

The friction torque test of thrust ball bearings was performed in the equipment shown in Fig. 5. The lower ring rotates with the hydraulic main shaft, and the upper ring matches the load block. When the bearing is running, the upper ring is dragged by the balls and drives the load to apply pressure to the force sensor. The computer calculates the collected force data as a torque value and stores them, with a data sampling frequency of 1 Hz. The data acquisition time of each experiment is 10 min.

2.3.3 *General test process*

The self-driving effect of bleed oil depends on two basic factors, one is the textured surface with self-driving function and the other is the presence of base oil. Therefore, wettability test of oil on GCr15 steel texture surface was designed first. Second, bearing vibration tests are carried out on four bearings prepared in Section 2.2. In this experiment, a relatively large axial load and a higher bearing

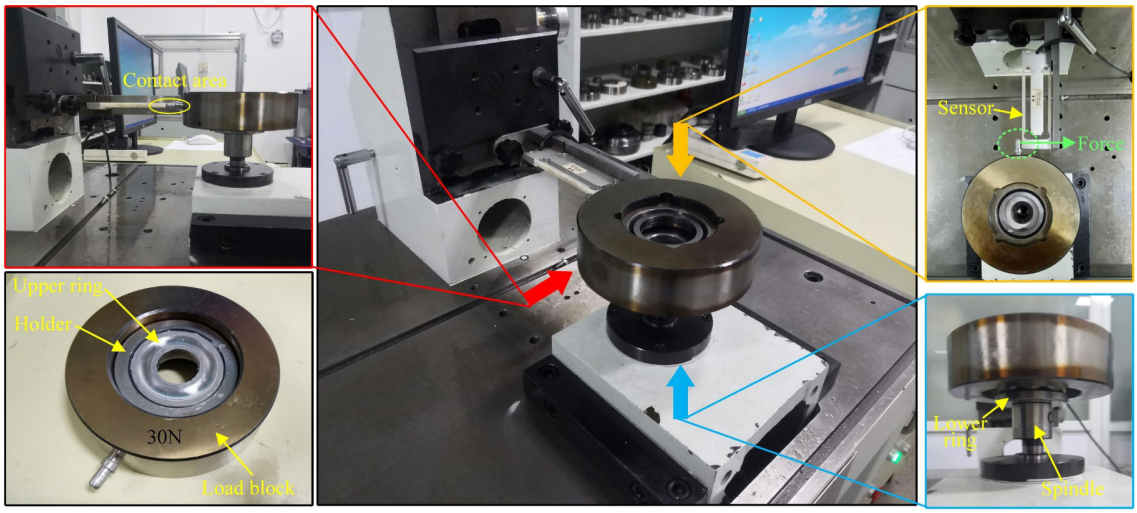

Fig. 5 Friction torque tester.

speed were set as the test conditions, which caused the grease to be fully sheared in the bearing operation, and the thickener fibers were broken, thus precipitating more bleed oil. Meanwhile, the friction generated more heat, which intensified the precipitation process. All these make the bearing guide surface contain sufficient bleeding oil, so that the microstructure with self-driving effect can play the effect of drainage and aggregation.

After that, bearing friction torque tests in low load condition were conducted twice on the bearings that have completed the vibration test. The first friction torque test was started directly without cleaning. At this point, the grease was sheared sufficiently and a large amount of base oil was precipitated. The friction torque of the test bearing was obtained under the drainage effect of self-driving textured guiding surface. Then the four sets of bearings were cleaned with petroleum ether and refilled with fresh greases. After a 2 min homogenizing grease process, the second friction torque test was carried out. In this test, the lubricating grease was not fully shear, the amount of base oil precipitation was less. And the friction torques of the bearings were measured under the condition that the micro-structure of the guiding surface existed but the self-driving effect of oil was not played. Figure 6 shows a complete experimental procedure of this study, which was conducted three times to ensure the reliability of the results. After the experiments, the upper ring was cut by wire cutting, and the wear condition of the raceway was observed by SEM.

3 Results and discussion

3.1 Wetting performance of textured surface

During the operation of grease lubricated ball bearings, the grease in the raceway is squeezed to both sides of the raceway by balls, and a large amount of grease is accumulated between the guiding surface and the surface of the cage. However, there is very little lubricant involved in lubrication at the bottom of the raceway, namely the roller/raceway contact area. Most grease lubricated rolling bearings will enter the starved condition after a period of operation. The existing research [27, 28] shows that the bleed oil is separated from the grease on both sides of the raceway by the extrusion of the balls to form a "lubricant reservoir" beside the contact area, which is an important component of bearing lubrication. The study of Scarlett [29] showed that the bearing life is greatly reduced when the grease is removed from the guiding surface on both sides of the raceway during the bearing operation. Therefore, we designed an oil droplet self-driven textured surface (Fig. 2(d)), which was set on the guiding surface of the bearing. It aimed to increase the backflow of bleed oil, thus suppressing the vibration and friction torque of the bearing. Meanwhile, two other types of textures as dimples

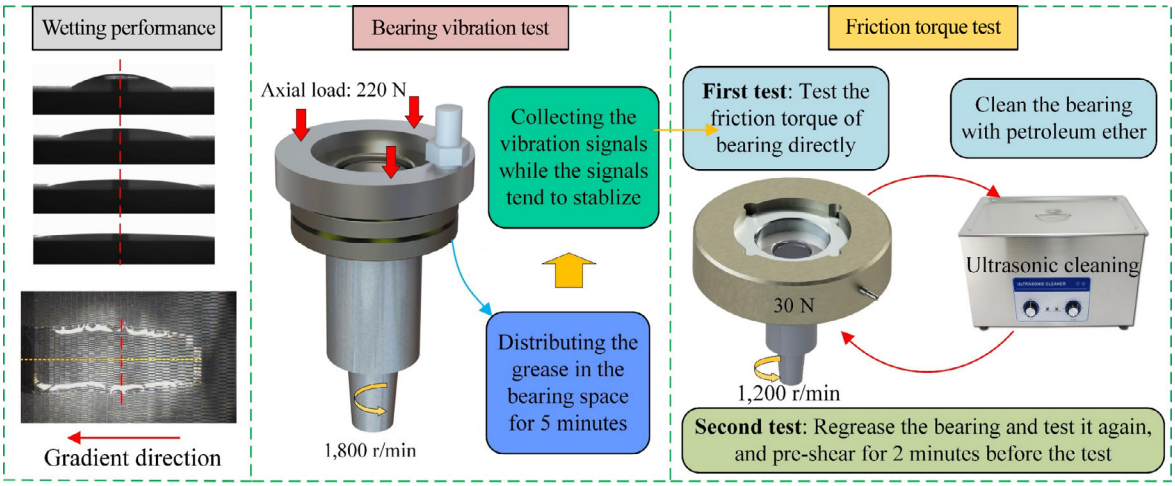

Fig. 6 Overview of experimental process.

and grooves were designed as comparison, as in Figs. 2(b) and 2(c).

In this part, we evaluated the spreading performance of PAO40 base oil on non-textured and three types of textured steel plates (GCr15) respectively.

As shown in Fig. 7, oil droplets almost do not diffuse on the non-textured steel plate, and the spreading of oil droplets from 1 s to 5 min did not change significantly.

The diffusion of oil droplets on dimple textured surface is also not obvious. However, due to the adsorption of the dimples on the oil droplets, the further spread of the oil is hindered, which makes the oil droplets form a hexagonal shape on the dimple textured surface.

When the oil droplet contacted uniform groove textured surface, it could spread rapidly along the direction of grooves. As can be seen from Fig. 7 that the left (groove-L) and right (groove-R) spreading distance of the oil droplet were close to the same until the oil reached the edge of the textured area. In addition, the width of the droplet in the vertical groove direction hardly changed during this period. Subsequently, due to the overflow from the textures, the oil then began to diffuse slowly in the direction perpendicular to the groove, and the width of oil droplet increased from 3.72 mm in 20 s to 4.65 mm in 5 min. Many studies have shown that the grooved texture can create a priority direction (parallel to the groove) for the diffusion of liquid [30], which limits the spreading of droplets in the vertical direction of the groove.

When oil droplet was placed on the gradient grooved surface, it rapidly diffused along the gradient direction without any external influence. In the opposite direction of the gradient, the edge of the oil droplet was pinned when it reached a larger spacing position. Furthermore, the spreading distances on the left (gradient groove-L) and right (gradient groove-R) sides of the droplet gradually different. The oil droplet spread continuously to the area with high texture density, while it was pinned to stop spreading at 5 mm on the side of area with low texture density.

The wettability gradient could be obtained when textures are gradient changeable. The motion behavior of the droplet on the wetting gradient surface is mainly determined by the driving force F_d caused by the difference of free energy between the two sides of the droplet, the hysteresis force F_h caused by the contact angle hysteresis and the adhesion resistance F_η caused by the relative motion between the solid and liquid. Because the magnitude of adhesion resistance F_η is far less than the driving force and the lag force [31, 32], the influence of F_η would be ignored in the following analysis. In the spreading of oil droplets, F_d makes oil droplets tend to a more lipophilic area on the textured surface [23, 33], which can be expressed as

$$F_d = \pi R^2 \gamma_{lv} \frac{\mathrm{d}\cos\theta}{\mathrm{d}y} = \pi R^2 \gamma_{lv} \frac{\mathrm{d}\cos\theta}{\mathrm{d}\theta} \frac{\mathrm{d}\theta}{\mathrm{d}y} = \pi R^2 \gamma_{lv} k \sin\theta \quad (1)$$

where R is the contact radius in the direction perpendicular to the gradient, γ_{lv} is the surface tension of the oil, θ is the sessile contact angle of oil droplets along the wettable gradient direction (y direction), dy is the integrating variable along y direction, k is equal to $-\mathrm{d}\theta/\mathrm{d}y$. According to Eq. (1), for a given R, it can be inferred that an increasing k or θ leads to a larger F_d. It is well known that due to the hysteresis of contact angle, the hysteresis force F_h is always opposite to the motion direction, as described in Ref. [34]:

$$F_h = 2R\gamma_{lv}(\cos\theta_{ao} - \cos\theta_{ro}) \quad (2)$$

where θ_{ao} and θ_{ro} correspond to the advancing and receding contact angles on the different area of gradient groove textured surface.

From the above analysis, the length of the grooves designed in this study is gradually shortened in the gradient direction, which makes k and F_W gradually increase. In addition, the higher the density of textures on the steel plate is, the larger F_d at the corresponding position is. When F_d is bigger than F_h, the oil droplet can spread in the gradient direction. In the lower density region, oil droplet is pinned when F_d is less than F_h.

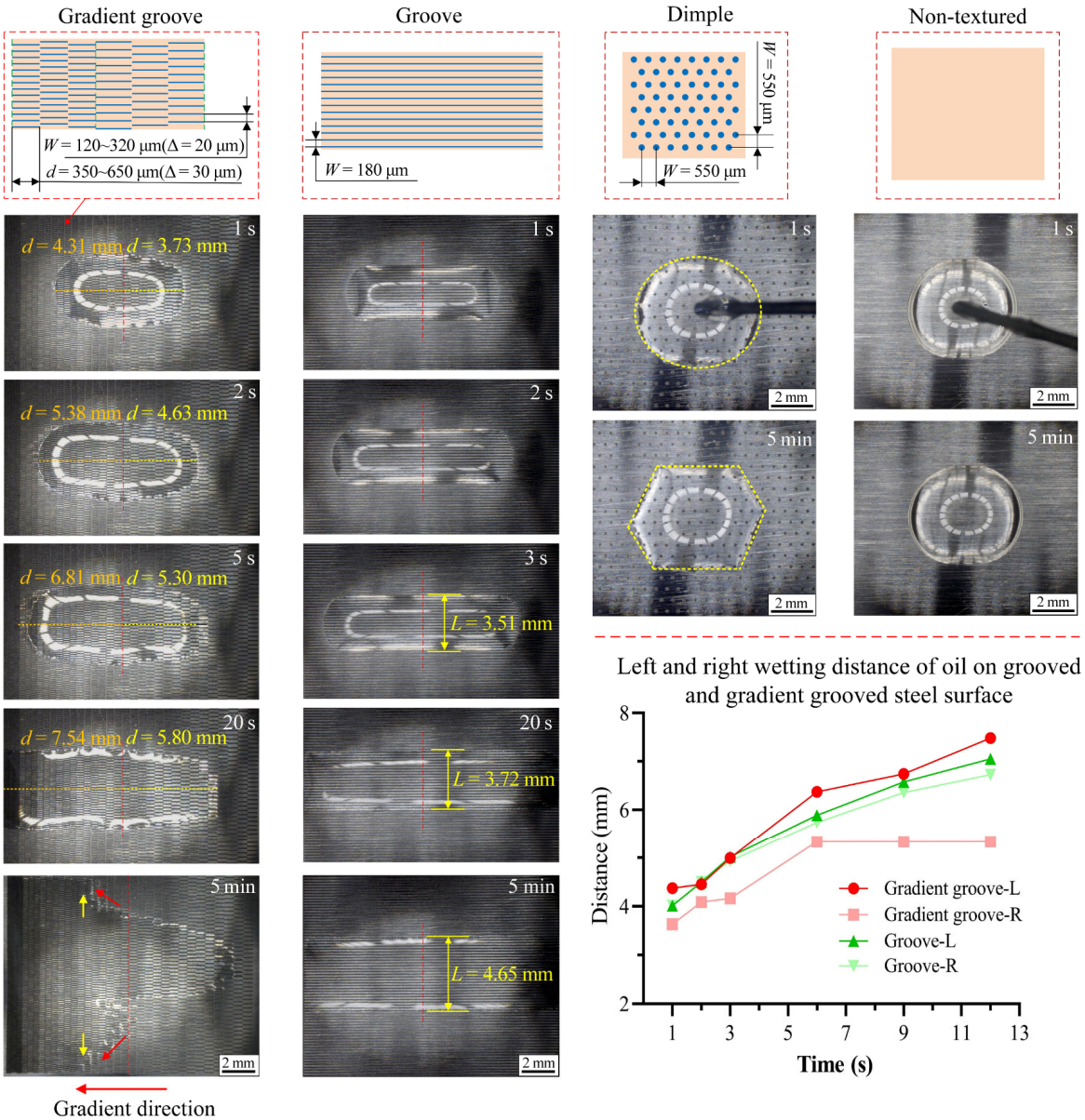

Fig. 7 Oil droplet spreading pattern.

Figures 8 and 9 show the wettability of four surfaces for PAO40 and their contact angle along with time, respectively. The contact angles of the oil droplets on the plain steel plate and the dimple textured surface quickly entered the equilibrium state, and their contact angles decreased from 58.1° to 35.6° and from 57.4° to 30.1° within 1 s, respectively. The contact angle of the oil droplets on the groove textured surface always kept a decreasing trend in 3 s (as shown in Fig. 9(c)), from 42.9° to 14°. At 30 s, the oil droplets spread completely, and the contact angle tends to 0°.

On the gradient grooved surface, the contact angle of the oil droplets also kept a decreasing trend in 3 s (as shown in Fig. 9(d)). And the dynamic contact angles θ_a (left side of the droplet) and θ_b (right side of the droplet) of the oil droplets always kept a difference of about 4° during the spreading process, with θ_a decreasing from 30.9° to 13.46° and θ_b decreasing from 22.7° to 9.3°. Due to the wettability gradient, the oil droplets spread faster towards a dense textured region, which is manifested macroscopically as a spontaneous unidirectional flow of oil droplets.

The experiments show that the isotropic non-textured steel plate and dimpled steel surface have large contact angles, while the anisotropic grooved and gradient grooved surfaces have smaller wetting angles in the groove direction, i.e., better spreading effects. So the grooves on the guiding surface as described in Section 2.2 enables the oil droplets to spread more easily in the radial direction of the bearing. Further, the unidirectional spreading guide effect of the gradient grooved surface can gather the oil droplets to the edge of the raceway and improve the raceway's ability to obtain bleed oil.

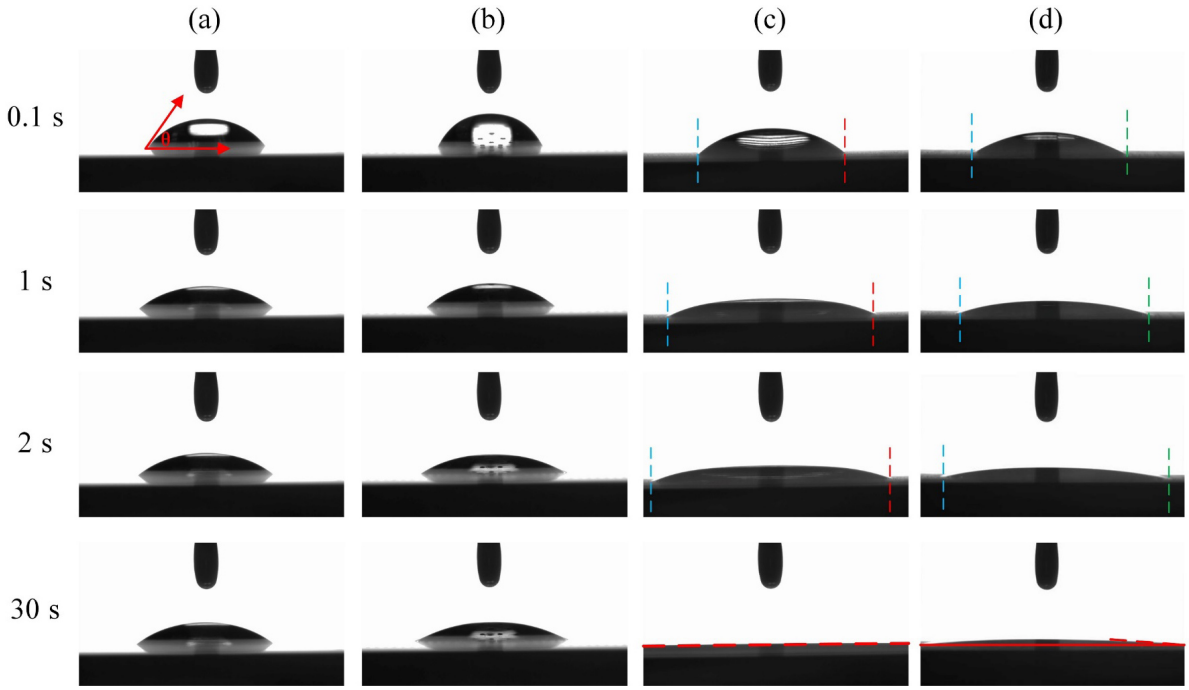

Fig. 8 Wettability of four surfaces for PAO40. (a) NB, (b) DB, (c) GB, and (d) GGB.

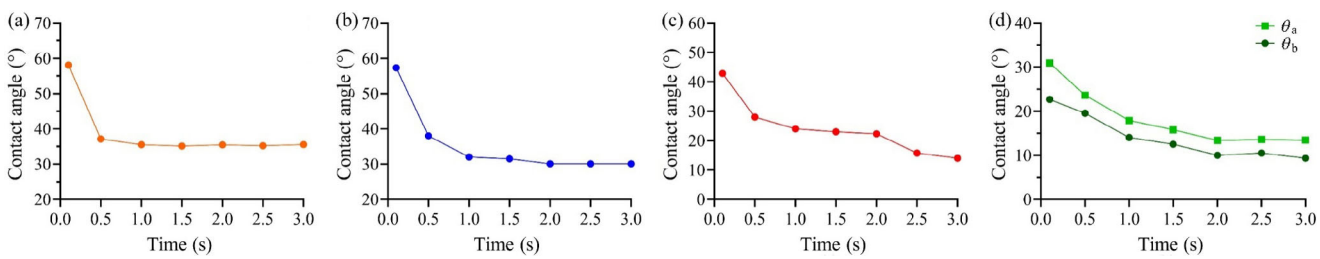

Fig. 9 Contact angle of four surfaces. (a) NB, (b) DB, (c) GB, and (d) GGB.

3.2 Bearing vibration performance

In order to analyze the effect of different types of textures on the vibration of the thrust ball bearings, the root mean square (RMS) and Kurtosis curves of the axial acceleration signals of the four bearings along with time were evaluated, as shown in Fig. 10. The RMS values characterize the overall vibration energy in the signals, while the kurtosis is a response to the shock characteristics.

As shown in Fig. 10(a), the RMS of NB is the largest and tends to decrease gradually during the whole experiment. This is because the bleed oil is slowly released by the shear extrusion of the grease in the raceway and the bearing lubrication is improved.

The RMS value of GB ranked second. The RMS decreased by 16.9% at the end of the test compared with NB. And the RMS curve almost stabilized after 7 min. According to Section 3.1, the spreading of base oil on uniform groove textured surface is bi-directional, as the direction of grooves on the guiding surface is the radial direction of the bearing, part of the oil can flow to the raceway, while the other part is spread and lost away from the raceway.

The RMS values of DB and GGB ranked third and fourth, respectively. Their trends are quite different from those of NB and GB. Within 10 min, the curves basically present a stable state without any obvious decline. It can be speculated that the texture on the guiding surface promotes the replenishment of the oil to the raceway, which makes the contact area fully supplied with oil and the bearings quickly enter the lubrication equilibrium state. In addition, the RMS values of DB and GGB decreased by 33.1% and 49.1% compared with NB at the end of the test. Section 3.1 shows that the dimpled texture can adsorb the oil to prevent it from spreading, which hinders the loss of bleed oil from the guiding surface of DB, thus improving the probability of the raceway getting oil. The best vibration performance of GGB is because there are more grooves on the GGB guiding surface near the two sides of the raceway and fewer grooves on the outer side. Thus, more bleed oil is attracted to the edge of the raceway and enters the raceway under the effect of the wetting gradient to improve the lubrication condition.

Kurtosis is the response to the impact characteristics of vibration signals [35], and the kurtosis of the normal distribution is equal to 3. When the kurtosis of bearing vibration deviates from 3, it indicates that the mechanical impact between the rolling body and the raceway is large. As shown in Fig. 10(b), the kurtosis value of NB is about 4 at the end of the experiment. And that of GB only slightly decreased compared with NB in the whole experiment process. The kurtosis values of DB and GGB are relatively close, and about 3. They are decreased by 26.8% and 24.6% compared with NB, respectively. It can be deduced that there is more bleed oil in those two bearing raceways, which plays a buffer and isolation role in the collision and friction vibration of the rolling body/raceway, thereby reducing the impact of the bearing vibration.

In the frequency domain, Fig. 11 shows the power spectral density (PSD) of four test bearings' vibration acceleration signals at the end of the test. In this experiment, the bearing acceleration signal shows typical broadband excitation. According to ISO15242-1:2015,

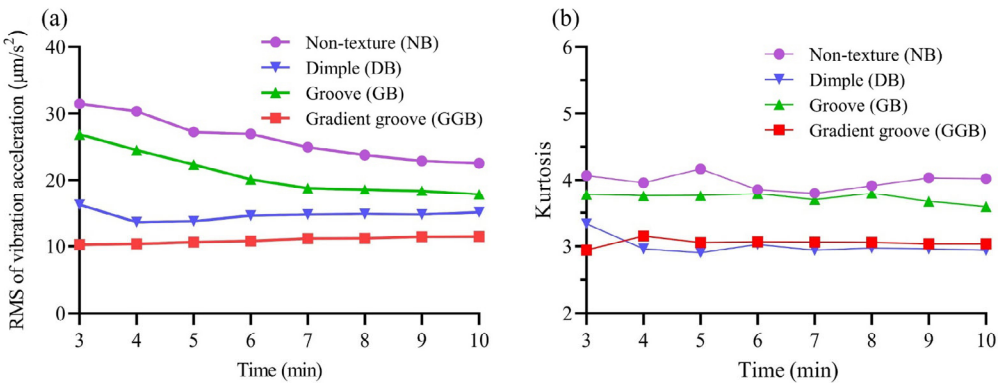

Fig. 10 RMS value and kurtosis of vibration acceleration of four bearings.

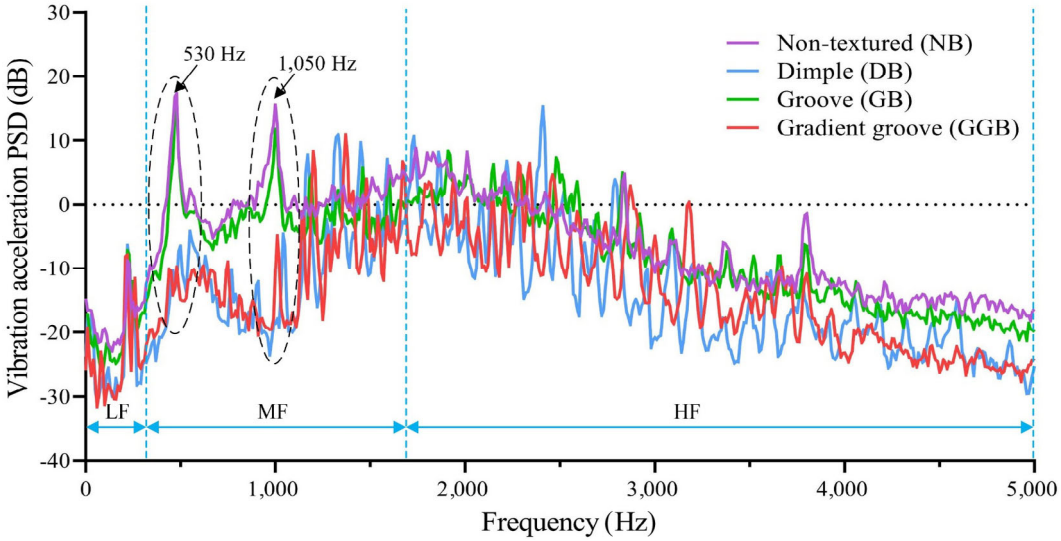

Fig. 11 PSD of vibration acceleration of four bearings.

the bearing acceleration vibration signal is divided into low-frequency band (50–300 Hz), medium-frequency band (300–1,800 Hz), and high-frequency band (1,800–10,000 Hz).

The power distribution of the four bearings in the low-frequency band is pretty low. In the middle-frequency band, NB and GB have two high power peaks at about 530 and 1,050 Hz, respectively. However, the vibration power of DB and GGB is significantly suppressed here. To further explore the energy distribution of vibration signals in each frequency band, RMS values of four bearings in three frequency bands were calculated. As shown in Fig. 12, the vibration signal of GB is lower than that of NB in the middle-frequency band as well as the high-frequency band. DB has a more significant reduction than that of GB. The RMS of GGB decreased most in the middle and high frequency bands, 65.3% and 48%, respectively. According to previous study [36], the low-frequency, medium-frequency, and high-frequency vibration of the bearing is mainly determined by the geometrical morphology, the waviness and the surface roughness of the raceway, respectively. Serrato et al. [37] reported that the changes in lubrication condition of a rolling bearing mainly affect its vibration in 600–10,000 Hz, and the reduction of oil film could cause the small impact among metallic surface irregularities (roughness/waviness), which increase the bearing vibration,

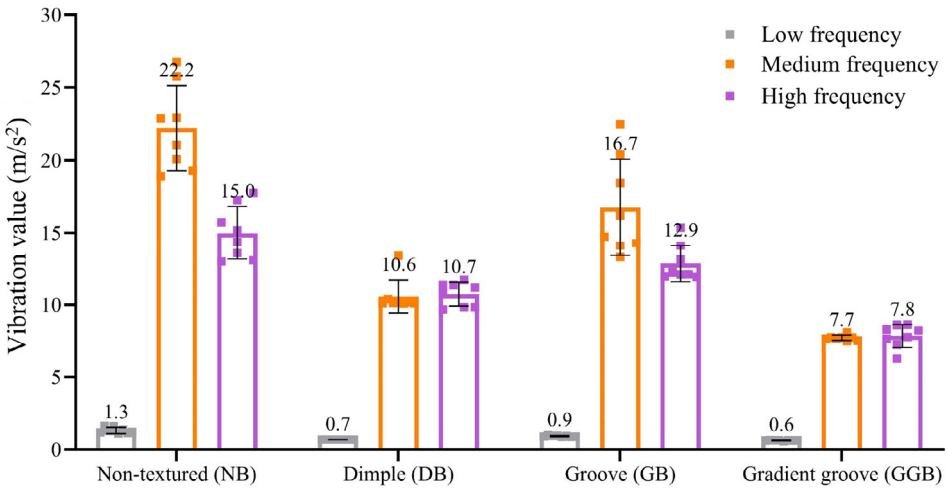

Fig. 12 RMS value of bearing vibration in different frequency band.

especially in medium and high frequency bands. This is consistent with our experimental results.

The grease distribution on the bearing raceway and the guiding surface after the test was photographed. As shown in Fig. 13(a), the grease on the guiding surface without texture is unevenly distributed and has less retention, which is owing to the weak adhesion of the metal surface to the grease. From a larger view, the grease in the NB raceway was almost exhausted after the experiment. The grease fingers were very thin, and only the light main finger could be seen. In comparison, the DB and GB's guiding surfaces have more grease residues, covering most of the guiding surface. At the same time, there are obvious grease fingers in the bearing raceway. In addition to the main grease finger, the slender fibrous bifurcation begins to appear (Figs. 13(b) and 13(c)). For GGB (Fig. 13(d)), there is a large amount of residual grease on the guiding surface, showing a relatively obvious accumulation, and there are a large number of stout and abundant grease fingers on the bearing raceway surface, which can effectively improve the lubrication state of the contact area [28].

Usually, a large amount of grease in the bearing raceway would be extruded by the rolling body to the guiding surface. Scarlett's research [29] shows that the grease on the guiding surface could reduce the escape of lubricant from the bearing raceway, and provide less base oil to the raceway. In this study, on one hand, the micro-structure on the guiding surface can increase the adhesion of grease, which can restrain the loss of lubricant compared with non-textured guiding surface. Experimental results also show that the vibration of three textured bearings is reduced. On the other hand, the wetting performance of textured surface in Section 3.1 shows that compared with DB and GB, the gradient grooved guiding surface of GGB has a self-driven effect on oil, and the high-density textured area near the edge of the raceway is more likely to accumulate base oil and thus enhance the bearing raceway's ability to obtain lubricant.

Combining bearing vibration and grease distribution, it can be indicated that the textured guiding surface could improve the content of bleeding oil in the raceway, increase the oil film thickness in the contact area, and reduce the collision probability of the metal surface, thus restraining the medium and high frequency vibration caused by waviness and roughness of raceway.

3.3 Friction torque performance

Friction torque is another important index of rolling bearing. Low friction torque can reduce the wear of bearing and prolong the service life of bearing. The friction torque of rolling bearing is directly related to the lubrication state of the contact area. Therefore, the improvement of contact supplement and contact starvation [38] of the lubricant between the rolling body and the raceway can reduce the friction torque of the bearing. This paper focuses on the influence of

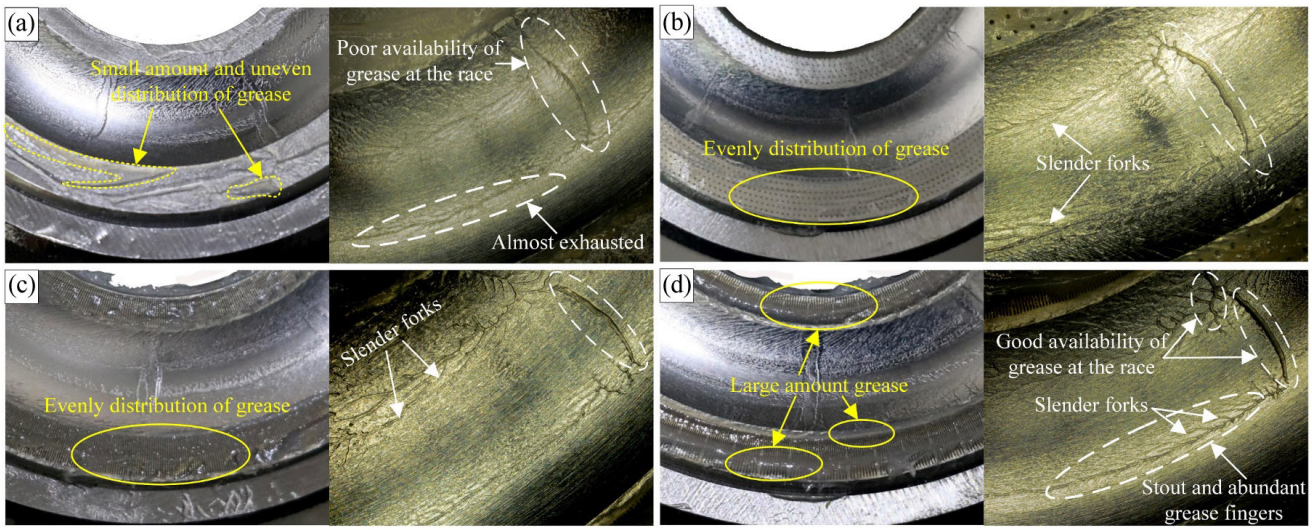

Fig. 13 Distribution of grease on guiding surface and raceway. (a) Non-textured, (b) dimple, (c) groove, and (d) gradient groove.

the textured guiding surface on the oil supply of rolling bearings, so the rotating speed and load are used as fixed parameters at a load of 30 N and a speed of 1,200 r/min.

Figure 14(a) shows the friction torque of bearings after the vibration test. At this time, the grease in the bearing had been sufficiently sheared, and the test results show that the ranking of each bearing friction torque is the same as the RMS of vibration signal ranking. Compared with NB, GGB has the largest reduction in friction torque of 10.5%. DB and GB also have a reduction of 7.9% and 4%, respectively. Thus, the texture on the guiding surface also has a positive effect on the bearing friction torque, increasing the amount of grease on the guiding surface and making it easier for the bleed oil precipitated from this part of the grease to flow back and replenish the bearing raceway. Especially for GGB, the driving force caused by the gradient grooves makes the bleed oil flow back towards the bearing raceway, which reduces the friction torque substantially. Relevant studies show that grease-lubricated bearings exhibit high friction torques under boundary lubrication or starvation mixed lubrication [39]. When the lubricant supply is sufficient, the bearings could be in mild mixed lubrication state, enabling the friction torque to be greatly reduced. This conclusion is consistent with the experimental results of this study.

Figure 14(b) shows the friction torque of the same group of bearings after cleaning and re-greasing. The friction torque differs less among the bearings, and only the GGB friction torque has a small reduction compared to the NB. Because the axial load was only 30 N and the vibration test had not been operated under the large load of 220 N, the grease is not sufficiently sheared, which leads to the oil precipitation is far less than the first test conditions. Therefore, the effect of textured guiding surface on the reduction of bearing friction torque is not obvious. It is proved from another aspect that the reduction of friction torque in the first test is caused by the backflow of bleed oil.

Figure 15 shows the SEM images of the four tested bearing raceway after the test and that of the pre-test bearing raceway. It can be seen that after three times of bearing vibration test and three times of friction torque test, the raceway surface of NB has deep scratches and obvious pits (Fig. 15(a)). Compared with the pre-tested bearing (Fig. 15(e)), the scratch of the raceway surface is significantly rougher and deeper. It can be inferred that the bearing was in a poor lubrication condition during the whole experiment, and the adhesive wear between the steel ball and raceway caused fatigue and thermal damage to the metal surface, which would significantly reduce the bearing service life. As shown in Fig. 15(b), DB has less corrosions/burns on the raceway surface, but deep grooves still exist. Compared with Fig. 15(a), the scratches on the raceway surface are relatively shallow. It can be seen from Fig. 15(c) that there are many pitting corrosions on the surface of GB raceway. The surface quality is similar to NB, indicating that grooved textured guiding surface has little improvement on bearing raceway surface damage. Figure 15(d) shows that GGB has the best raceway surface quality, with fine and shallow scratches, and no obvious burns, which proves that the bearing was adequately lubricated, allowing sufficient base oil to effectively isolate the contact area, delaying metal fatigue and reducing surface scratches.

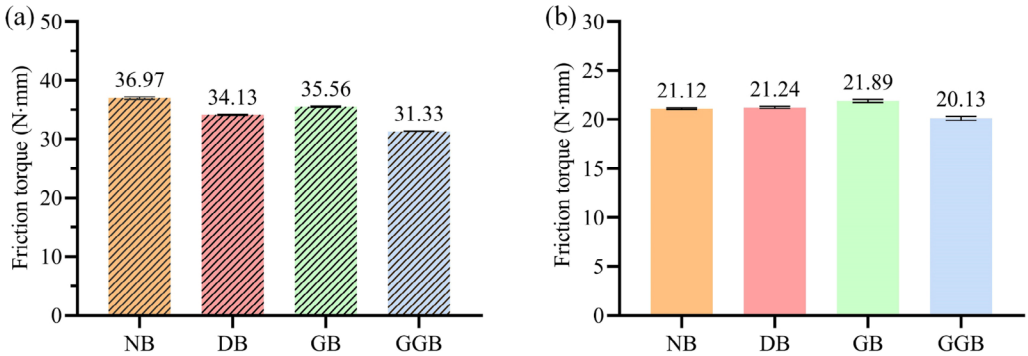

Fig. 14 Friction torque. (a) Bearings after the vibration test and (b) bearings after cleaning and re-greasing.

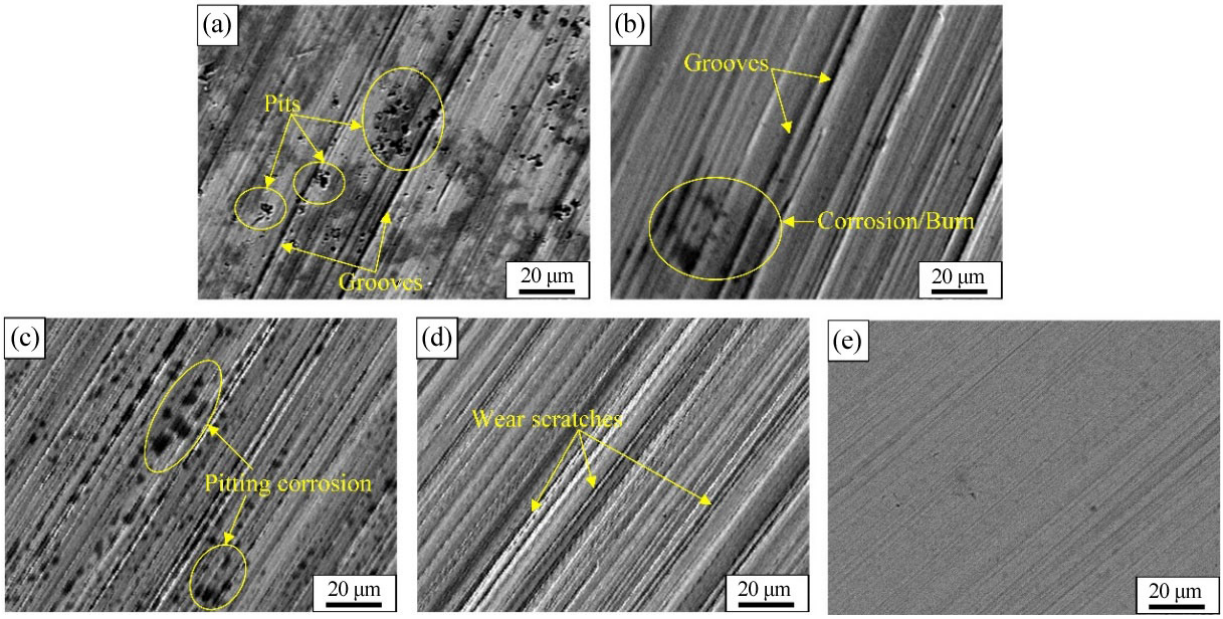

Fig. 15 SEM images of bearing raceways. (a) Non-textured, (b) dimple, (c) groove, (d) gradient groove, and (e) pre-tested.

4 Conclusions

In this paper, the improvement of lubrication condition by textured guiding *z* of the thrust ball bearing is investigated. Taking the non-textured thrust ball bearing as a comparison, the vibration and friction torque of the bearing with dimples, uniform groove, and gradient groove textured guiding surface are tested, respectively. The following conclusions were obtained.

1) The wettability gradient could be obtained when textures are gradient changeable. Thus, the gradient groove textured surface has a unidirectional guiding effect on oil droplets, which is macroscopically manifested as directional self-driving of oil droplets. The uniform groove textured surface enables the oil droplets to spread rapidly and over long distances along the groove direction, but does not provide one-way guidance. The dispersed dimples have adsorption effect on oil droplets, which can enhance the adhesion ability of oil droplets on the textured surface, but the spreading range of droplets is small.

2) The textures on the guiding surface can enhance the oil content in the bearing raceway, which provides good damping in the contact area and can effectively reduce bearing vibration. Among the three types of textured bearing, the gradient grooved bearing (GGB) has the best damping effect. The vibration acceleration root mean square (RMS) of GGB is reduced by 49.1% and the kurtosis is reduced by 24.6% compared with the non-textured bearing (NB). In addition, frequency domain analysis shows that the backflow of separated oil mainly inhibits the vibration energy of thrust ball bearings in middle and high frequency bands. GGB's RMS in the middle and high band decreased the most, reaching 65.3% and 48% respectively.

3) When the grease is fully sheared, the gradient groove textured surface has obvious effect on the oil drainage, which can effectively improve the bearing lubricated condition and reduce the bearing friction torque. Compared with NB, the GGB friction torque is reduced by 10.5%. In addition, the enhancement of bearing lubrication by gradient groove textures can significantly delay metal fatigue and reduce raceway surface scratches.

Acknowledgements

This work was supported by National Key R&D Program of China (Grant No. 2020YFB2006803), the Fundamental Research Funds for the Provincial Universities of Zhejiang (Grant No. GK209907299001-006), Natural Science Foundation of Zhejiang Province (Grant No. LY19E050014), and Foundation of Zhejiang

Provincial Education Department of China (Grant No. Y202044314).

References

[1] Lugt P M. A Review on grease lubrication in rolling bearings. *Tribol T* **52**(4): 470–480 (2009)

[2] Li X M, Guo F, Poll G, Fei Y, Yang P. Grease film evolution in rolling elastohydrodynamic lubrication contacts. *Friction* **9**(1): 179–190 (2021)

[3] Gonçalves D E P, Campos A V, Seabra J H O. An experimental study on starved grease lubricated contacts. *Lubricants* **6**(3): 82 (2018)

[4] Huang L, Guo D, Wen S Z, Wan G T Y. Effects of slide/roll ratio on the behaviours of grease reservoir and film thickness of point contact. *Tribol Lett* **54**: 263–271 (2014)

[5] Kasem H, Shriki H, Ganon L, Mizrahi M, Abd-Rbo K, Domb A J. Rubber plunger surface texturing for friction reduction in medical syringes. *Friction* **7**(4): 351–358 (2019)

[6] Zhang K D, Deng J X, Xing Y Q, Li S P, Gao H H. Effect of microscale texture on cutting performance of WC/Co-based TiAlN coated tools under different lubrication conditions. *Appl Surf Sci* **326**: 107–118 (2015)

[7] Amini S, Hosseinabadi H N, Sajjady S A. Experimental study on effect of micro textured surfaces generated by ultrasonic vibration assisted face turning on friction and wear performance. *Appl Surf Sci* **390**: 633–648 (2016)

[8] Vladescu S C, Fowell M, Mattsson L, Reddyhoff T. The effects of laser surface texture applied to internal combustion engine journal bearing shells—An experimental study. *Tribol Int* **134**: 317–327 (2019)

[9] Fowell M T, Medina S, Olver A V, Spikes H A, Pegg I G. Parametric study of texturing in convergent bearings. *Tribol Int* **52**: 7–16 (2012)

[10] Tala-Ighil N, Fillon M, Maspeyrot P. Effect of textured area on the performances of a hydrodynamic journal bearing. *Tribol Int* **44**: 211–219 (2011)

[11] Ye S G, Tang H S, Ren Y, Xiang J W. Study on the load-carrying capacity of surface textured slipper bearing of axial piston pump. *Appl Math Model* **77**: 554–584 (2020)

[12] Marian V G, Kilian M, Scholz W. Theoretical and experimental analysis of a partially textured thrust bearing with square dimples. *P I Mech Eng J-J Eng* **221**: 771–778 (2007)

[13] Bhardwaj V, Pandey R K, Agarwal V K. Experimental investigations for tribo-dynamic behaviours of conventional and textured races ball bearings using fresh and MoS_2 blended greases. *Tribol Int* **113**: 149–168 (2017)

[14] Vidyasagar K E Ch, Pandey R K, Kalyanasundaram D. An exploration of frictional and vibrational behaviors of textured deep groove ball bearing in the vicinity of requisite minimum load. *Friction* **9**(6): 1749–1765 (2021)

[15] Hsu C J, Stratmann A, Medina S, Jacobs G, Mücklich F, Gachot C. Does laser surface texturing really have a negative impact on the fatigue lifetime of mechanical components? *Friction* **9**(6): 1766–1775 (2021)

[16] Lu Y, Sathasivam S, Song J, Crick C R, Carmalt C J, Parkin I P. Robust self-cleaning surfaces that function when exposed to either air or oil. *Science* **347**: 1132 (2015)

[17] Xu Y, Zhang J, Xuan Y, Wang J, Meng F. Synergetic or colliding effects on the solar-electric conversion efficiency from light-trapping structured surfaces: Coupling optical-electrical features of bifacial solar cells. *Solar Energy* **207**: 517–527 (2020)

[18] Yuan Z, He Y, Lin C C, Liu P, Cai K Y. Antibacterial surface design of biomedical titanium materials for orthopedic applications. *J Mater Sci Technol* **78**: 51–67 (2021)

[19] Ishizaki T, Hieda J, Saito N, Saito N, Takai O. Corrosion resistance and chemical stability of super-hydrophobic film deposited on magnesium alloy AZ31 by microwave plasma-enhanced chemical vapor deposition. *Electrochim Acta* **55**: 7094–7101 (2010)

[20] Deng S Y, Shang W F, Feng S L, Zhu S P, Xing Y, Li D, Hou Y P, Zheng Y M. Controlled droplet transport to target on a high adhesion surface with multi-gradients. *Sci Rep* **7**: 45687 (2017)

[21] Li J Q, Zhou X F, Li J, Che L F, Yao J, McHale G, Chaudhury

M K, Wang Z K. Topological liquid diode, *Sci Adv* **3**(10): 3530 (2017)

[22] Liu C R, Sun J, Li J, Xiang C H, Che L F, Wang Z K, Zhou X F, Long-range spontaneous droplet self-propulsion on wettability gradient surfaces. *Sci Rep* **7**: 7552 (2017)

[23] Chen X Z, Li X, Zuo P, Li X J, Liang M S, Sun J X, Wang M M, Wang S M, Jiang L. Controllable fabrication of unidirectional liquid spreading surface through confining plasma eruption and femtosecond laser double pulses. *Appl Surf Sci* **504**: 144110 (2020)

[24] Li J, Qin Q H, Shah A, Ras R H A, Tian X L, Jokinen V. Oil droplet self-transportation on oleophobic surfaces. *Sci Adv* **2**: 1600148 (2016)

[25] Liu C L, Guo F, Wong P, Li X M. Laser pattern-induced unidirectional lubricant flow for lubrication track replenishment. *Friction* **10**(8): 1234–1244 (2022)

[26] Fan X Q, Li W, Li H, Zhu M H, Xia Y Q, Wang J J. Probing the effect of thickener on tribological properties of lubricating greases. *Tribol Int* **118**: 128–139 (2018)

[27] Huang L, Guo D, Liu X, Xie G X, Wan G T Y, Wen S Z, Effects of nano thickener deposited film on the behaviour of starvation and replenishment of lubricating greases. *Friction* **4**(4): 313–323 (2016)

[28] Huang L, Guo D, Wen S Z. Starvation and reflow of point contact lubricated with greases of different chemical formulation. *Tribol Lett* **55**: 483–492 (2014)

[29] Scarlett N A, Paper 21: Use of Grease in Rolling Bearings, Proceedings of the Institution of Mechanical Engineers. *Conference Proceedings* **182**: 585–624 (1967)

[30] Chen Y, He B, Lee J H, Patankar N A. Anisotropy in the wetting of rough surfaces. *J Colloid Interf Sci* **281**: 458–464 (2005)

[31] Daniel S, Chaudhury M K. Rectified motion of liquid drops on gradient surfaces induced by vibration. *Langmuir* **18**: 3404–3407 (2002)

[32] Suda H, Yamada S. Force measurements for the movement of a water drop on a surface with a surface tension gradient. *Langmuir* **19**: 529–531 (2003)

[33] Hou Y P, Peng S L, Dai L M, Zheng Y M. Droplet manipulation on wettable gradient surfaces with micro-/nano-Hierarchical structure. *Chem Mater* **28**: 3625–3629 (2016)

[34] Daniel S, Sircar S, Gliem J, Chaudhury M K. Ratcheting motion of liquid drops on gradient surfaces. *Langmuir* **20**: 4085–4092 (2004)

[35] Xue Y, Shi X, Zhou H, Lu G, Zhang J. Effects of groove-textured surface combined with Sn–Ag–Cu lubricant on friction-induced vibration and noise of GCr15 bearing steel. *Tribol Int* **148**: 106316 (2020)

[36] Wu C, Xiong R F, Ni J, Teal P D, Cao M L, Li X L. Effect of grease on bearing vibration performance caused by short-time high-temperature exposure. *J Braz Soc Mech Sci Eng* **42**: 69 (2020)

[37] Serrato R, Maru M M, Padovese L R. Effect of lubricant viscosity grade on mechanical vibration of roller bearings. *Tribol Int* **40**(8): 1270–1275 (2007)

[38] Cann P M. Starved grease lubrication of rolling contacts. *Tribol T* **42**: 867–873 (1999)

[39] Vengudusamy B, Enekes C, Spallek R. On the film forming and friction behaviour of greases in rolling/sliding contacts. *Tribol Int* **129**: 323–337 (2019)

Can WU. He received his B.S. and Ph.D. degrees majoring in mechanical design and theory from Zhejiang University, China, in 2005 and 2010, respectively. He joined Hangzhou Dianzi University since 2010. His current position is an associate professor at the School of Mechanical Engineering of Hangzhou Dianzi University. His research areas cover tribology, lubricants, surface interface technology, and dynamics of rolling bearing.

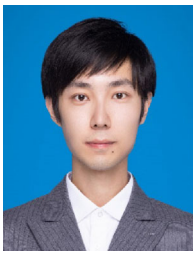

Kai YANG. He received his B.S. degree in mechanical design and automation from Shenyang Aerospace University, China, in 2016. He got his M.S. degree in mechanical engineering from Hangzhou Dianzi University, China, in 2022. His research interest focuses on the tribology, textured surface, and dynamic analysis of rolling bearing.

Jing NI. He received his M.S. and Ph.D. degrees in mechanical and engineering from Zhejiang University, China, in 2003 and 2006 respectively. He joined Hangzhou Dianzi University since 2006. His current position is a full professor and dean of the School of Mechanical Engineering of Hangzhou Dianzi University. His research areas cover lubrication materials, surface interface technology, ultra-precision machining, machining dynamics, etc.